Talanta 83 (2010) 197–204

Contents lists available at ScienceDirect

Talanta

journal homepage: www.elsevier.com/locate/talanta

Electrodeposited silver nanodendrites electrode with strongly enhanced electrocatalytic activity

B. Rezaei *, S. Damiri

Department of Chemistry, Isfahan University of Technology, Isfahan 84156-83111, Islamic Republic of Iran

ARTICLE INFO

Article history:
Received 25 August 2010
Received in revised form 6 September 2010
Accepted 6 September 2010
Available online 21 September 2010

Keywords:
Silver nanodendrites
Electrodeposition
Soft template
Electrocatalyst
Multiwalled carbon nanotubes
Electrochemical impedance spectroscopy

ABSTRACT

Highly uniform dendritic silver nanostructures as a new electrode material, have been synthesized by electrodeposition on the glassy carbon (GC) electrode with assistance of polyethylene glycol 400 (PEG-400) as a soft template, to achieve a superior electrocatalyst with enhanced detection sensitivity in electroanalysis compared to conventional bulk Ag electrodes. The effects of the growth conditions such as concentrations of the reagents and applied potentials on the morphology and structure of as-prepared tree-like nanostructures have also been investigated by scanning electron microscopy (SEM), atomic force microscopy (AFM) and X-ray diffraction (XRD). In the silver nanodendrites (AgNDs), the diameter of the trunk is around 100–200 nm with length up to 10–40 μm, and the length of its branches can reach 10 μm. In addition, the electrocatalytic behavior of this modified electrode was exploited as a sensitive detection system for the reduction of RDX high explosive, hydrogen peroxide and hexacyanoferrate (HCF) by cyclic voltammetry (CV) and electrochemical impedance spectroscopy (EIS) techniques. Also, the obtained results were compared to multiwalled carbon nanotubes (MWCNTs) and bulk silver electrodes. These studies show that the nanodendritic silvers significantly increase the electron-transfer rate of the electrochemical reactions by as much as 1–2 orders of magnitude.

1. Introduction

Nanotechnology has recently become one of the most exciting forefront fields in analytical chemistry and design of new useful electrocatalysts [1–3]. Beside of the development of ultrasensitive electrochemical sensors and need to miniaturization of sensing devices, various nanomaterials and nanostructures have drawn considerable attentions due to their unique size and properties. Therefore, traditional macroelectrodes are being replaced with their nanostructure analogues [4,5]. The predominant advantages of using nanostructure modified electrodes compared to typical macroelectrodes is their large effective surface area, considerable mass transport, high catalytic activity, and their ability to exert control over the local environment at the electrode surface [4,5]. The existing of very sharp edge sites and defects on the nanostructures, causes a suitable interaction between redox species with nanostructure modified electrode surface which is resulted to decrease overpotential of the electrochemical reactions to become more reversible than that displayed by the same material in a conventional form [6,7].

At the present time, micro/nanoscaled materials, due to their unique optical, electrical, magnetic, and catalytic properties are being synthesized and investigated for their potential application in various fields, such as electroanalysis [8,9], optoelectronics [10], energy generation/storage [11,12], and catalysis [13,14]. Recently, considerable efforts have been focused on the design, synthesis, and application of high ordered inorganic crystals with specific sizes, shapes, and hierarchies. Different kinds of nanomaterials, such as metals [3], semiconductors, oxides [14], and carbon nanotubes [15], and different nanostructures such as nanowire [16,17], flower-like [18,19], urchin-like [20], mushroom-like [21], and dendrite-like [22–26] have been reported based on different advanced strategies. Noble metal nanostructures have been the subject of most intensive research due to their novel properties and intriguing applications in different areas such as electronic, magnetic, catalysis, chemical and biological sensing, optical, micromechanical device and surface-enhanced Raman scattering (SERS) detection [27–31]. The intrinsic properties of metal nanostructures are determined by their size, shape, morphology, composition, and crystallinity [32–35]. Accordingly, silver has been extensively exploited in a variety of applications such as catalysis, through electronics, photonics and photography. Silver electrodes have a great importance in electroanalysis and sensing devices, and as yet they have been used to detect some important compounds such as hydrogen peroxide [36], L-cysteine [37], benzyl chloride [38], 6-mercaptopurine

* Corresponding author. Tel.: +98 311 3912351; fax: +98 311 3912350.
E-mail address: rezaei@cc.iut.ac.ir (B. Rezaei).

0039-9140/$ – see front matter © 2010 Elsevier B.V. All rights reserved.
doi:10.1016/j.talanta.2010.09.006

[39], enzyme [40], DNA [41], hemoglobin [42], and myoglobin [43].

The excellent nanodendritic structure of silver, as a new electrode material, has a very high specific surface area along with numerous active sites and sharp edges which can be promising its applications in the electrochemical systems. Since the discovery of carbon nanotubes, various nanoparticles [3,4] and nanostructure electrocatalysts such as nanotubes [6,44] nanowires [16,17,45,46], nanoflowers [47], nanorods [48,49] nanofiber [50], and porous structures [7] have been introduced as new valuable morphology of the electrode materials in the electrochemical sensors or other related applications [1], that improve significantly the sensing capability of the conventional macroelectrodes. In comparison to spherical particles, nanowires have recently attracted much attention, which own a number of unique physical and electronic properties that endow them new and important activities. Using of three-dimensional (3D) Ag nanodendrites with tree-like structures introduce a new attractive strategy for designing of the electrocatalyst morphologies and the modification of conventional electrodes that can be used in the electroanalysis or other electrochemical systems. Dendritic patterns are essential phenomena that are observed in non-equilibrium conditions for metallurgic, inorganic, and organic crystal growth; hence provide a natural framework for the study of disordered systems [51]. The diffusion-limited aggregation (DLA) model and the anisotropic crystal growth are widely used to explain and analyze these growth phenomena [52–56]. In the electrodeposition methods, some processes such as kinetic anisotropy in the reduction of Ag^+ ions [26] and the lack of electrolyte play an important role in the formation of Ag dendrites [57].

Up to now, a few methods have been exploited for the fabrication of noble metal dendrites including the electrochemical deposition, the irradiation reduction, the pulse sono-electrochemical technique, the ultrasonic-assisted solution reduction and the displacement reaction [24,54,58–62]. Many of these routes use water soluble polymers such as polyvinyl alcohol (PVA) and poly(vinyl pyrrolidone) (PVP) as protecting agents [54,61,62]. Ye et al. reported the fabrication of silver dendrites on silicon wafers via an electroless metal deposition technique [63]. A very interesting technique for the synthesis of silver dendrites by electrochemical deposition in aqueous solution at the presence of DNA was reported by Chen et al. [64]. Here, the dispersion property of DNA enhanced the stability of silver dendrites with the basic units of DNA interacting with the silver particles to enhance the surfactant properties. A mixed surfactant system of cetyltrimethylammoniumbromide (CTAB) and sodium dodecyl sulfate (SDS) was reported by Zheng et al. for synthesis of silver nanowires and dendrites in an aqueous medium [65]. Also, other strategies such as the electroreduction of $AgNO_3$ in ammoniacal solution [26], the electrodeposition with the assistance of triblock copolymer P123 [24], using a surfactant-free method by a suspension of zinc microparticles as a heterogeneous reducing agent [23], the replacement reaction in $AgNO_3$ aqueous solution [66] and a electrochemical synthesis on a Ni/Cu substrate with superhydrophobic surfaces [67] have been introduced for the preparation of tree-like Ag nanostructures.

This paper describes a simple and reliable electrochemical strategy for the modification of glassy carbon (GC) electrodes with silver nanodendrites to achieve a superior electrocatalyst with enhanced detection sensitivity in electroanalysis compared to conventional bulk Ag electrodes. Electrodeposition is an efficient method to synthesize new materials with high yields, and the nanoparticle shapes and sizes can be readily controlled by adjusting the preparation conditions [68]. Therefore, at first silver nanodendrites on GC electrode were prepared by means of electrodeposition technique at controlled potential conditions by employing polyethylene glycol-400 (PEG-400) as a soft template, and was discussed their morphology, structure, and formation mechanisms. Then, the electrocatalytic behavior of this modified electrode was evaluated by cyclic voltammetry (CV) and electrochemical impedance spectroscopy (EIS) techniques using hexacyanoferrate (HCF: $K_3Fe[CN]_6$), as an electrochemical probe, and these studies were compared to multiwalled carbon nanotubes modified GC and conventional bulk Ag electrodes. HCF is a substance that undergoes reversible electrochemical reaction on various electrodes and is widely used as an electrochemical probe to investigate the characteristics of films on electrode surfaces. Also, the reduction of some important compounds such as hydrogen peroxide and RDX (hexahydro-1,3,5-trinitro-1,3,5-triazine; also known as cyclonite or hexogen) high explosive was evaluated and compared to other electrodes. The detection of explosives and related compounds has received considerable attention for national security and environmental applications. RDX high explosive, similar to other nitramine materials, is mutagenic, toxic and has the tendency to persist in the environment [69]. Also, the detection and determination of hydrogen peroxide are of practical importance in chemical, biological, clinical, environmental and many other fields [36]. The Ag nanodendritic modified electrode was found to have very electrocatalytic behavior toward the reduction of mentioned compounds that make it ideal material for the fabrication of electrochemical sensors.

2. Experimental

2.1. Apparatus and reagent

2.1.1. Materials and chemicals

All chemicals, unless mentioned otherwise, were of analytical grade and were used as received. All aqueous solutions were made with demineralized water, which was further purified with a Milli-Q system (Millipore) with the resistivity not less than 18.0 MΩ at 25 °C. Universal buffer (boric acid, phosphoric acid, acetic acid and sodium hydroxide, 0.1 mol L^{-1}) solutions with different pH values were used for the study of the pH influence. The MWCNTs, bought from Iran's Research Institute of Petroleum Industry and synthesized by chemical vapor deposition (CVD), had a diameter of 8–15 nm, a length of ca. 50 μm and the purity of >95%.

2.2. Electrochemical measurements

Electrochemical measurements were carried out at room temperature in a conventional three-electrode cell, powered by an electrochemical system comprising the Autolab system with PGSTAT 12 and FRA2 boards (Eco Chemie B. V., Utrecht, Netherlands). The system was run on a PC using GPES and FRA 4.9 software. For impedance measurements, a frequency range of 100.0 kHz to 10.0 Hz was employed. The ac voltage amplitude used was 5 mV, and the equilibrium time was 10.0 min. Before each experiment, the solution was purged by nitrogen gas for 10.0 min.

The potentiostatic deposition of silver was accomplished by using a silver wire quasi-reference electrode (AgQRE) immersed directly in the silver plating solution, except for silver-free control experiments, which were performed by using a saturated Ag/AgCl electrode. A platinum wire counter electrode was employed for all experiments. The MWCNTs, similar to other reports, was pretreated in nitric acid solution [70], then it was abrasively immobilized on a preheated glassy carbon electrode (5 min at 50 °C) by gently rubbing of the electrode surface on a filter paper supporting the carbon nanotubes [71].

2.3. Preparation and characterization of silver nanodendrites

The electrodeposition of silver nanodendrites was carried out using an electrochemical cell test with a three-electrode configuration in the electrolyte. A planar glassy carbon electrode (GCE) was used as the working electrode, a platinum electrode, spaced with 15 mm from GCE, as the counter electrode, and a silver wire as a semi-reference electrode. Before electrodeposition process, the GCE was carefully polished with 5.0 μm alumina slurry on a polishing cloth, then washed ultrasonically in methanol and water, respectively. For the deposition, a chronoamperometry mode at the constant potential of −0.8 V vs. AgQRE for a period of 20.0 min was applied. Here, 0.02 mol L^{-1} silver nitrate (Aldrich, 99.999%) solution was prepared into a homodisperse mixture of PEG-400 (polyethylene glycol 400)/H_2O (1:1, v:v) and it was used as the electrodeposition electrolyte. After synthesis, the silver nanocrystals deposited on the working electrode were thoroughly washed with acetone droplets and water, and dried at 50 °C for 2 h.

The product was characterized by powder X-ray diffraction (XRD) on a Philips Xpert-MPD Model 3040 X-ray diffractometer equipped with Cu Kα radiation. Microscopic observation of the electrode surfaces was performed by an atomic force microscope (AFM) (DualScopeTM scanning probe-optical, DME model C-21, Denmark) in air. Average surface roughness of the samples and their density of summits were measured from height profile of AFM images using DME SPM software (version 2.1.1.2). Also, the scanning electron microscopy (SEM) images were recorded with a Philips XL Model 30 microscope.

2.4. Determination of the microscopic surface area of the electrodes by in situ voltammetric methods

For evolution of surface area of each used electrode in this research, e.g. MWCNs and AgNDs modified GC electrodes, and Ag electrode, it was used an individual electrochemical method for each case. The surface area of the conventional Ag electrode was calculated using the differential double layer capacitance (C_d) of the actual electrode surface, by assuming that the capacitance of the double layer for the polycrystalline silver electrode in 0.1 mol L^{-1} $HClO_4$ solution amounts to 28.0 μF cm^{-2} [72,73]. This metal shows a well-defined double layer region, and it is possible to estimate the pseudo-capacitance through the dependence of the capacitive current with the potential sweep rate. This method does not have a suitable efficiency for the determination of real surface area of AgNDs modified GCE. Thus we compared the amount of charge consumption for the reduction of 200.0 μmol L^{-1} RDX by cyclic voltammetry on the silver or AgNDs electrode in the conditions of 0.1 mol L^{-1} universal buffer with pH 7.0 and the scan rate of 100 mV s^{-1} for the estimation of microscopic surface area of modified electrode. The surface area of GC electrode was 0.0314 cm^2 and for the AgNDs modified electrode, the microscopic surface area was found nearly 3.44 times greater (0.1080 cm^2).

The microscopic area of the MWCNTs modified glassy carbon electrode was obtained by cyclic voltammetry using 1.0 mmol L^{-1} HCF as a probe [70]. The electroactive surface area of this modified electrode was about 1.15 times larger than the bare GC electrode.

3. Results and discussions

3.1. Morphological characterization of the prepared Ag nanodendrites electrode

Typical SEM images of the products exhibit that Ag crystals obtained under the mentioned experimental conditions possess a nanodendritic structure (see Fig. 1a–c). It can be observed that silver dendrites were obtained in a large quantity and good uniformity by this route. The individual Ag dendrites have two- and three-dimensional structures with one trunk (long axis) and branches (short axes). The nanorods in each branch are parallel to each other and in the same plane, and make an angle of about 60° with the trunk, which indicates that the Ag dendritic crystals grow along a preferential direction. The diameter of the trunks is around 200–300 nm and their length up to 10–40 μm. The length of the branches can reach 10 μm. More interestingly, during the growth process of silver nanocrystal, each branch can also be a trunk to support the growth of silver nanorods. Thus, the self-replication makes this kind of silver nanocrystal have a more advanced structure.

In Fig. 1d, it has been shown an XRD pattern of silver dendrites on the GCE support synthesized at 20.0 mmol L^{-1} silver nitrate for 20.0 min of electrodeposition time. The five diffraction peaks can

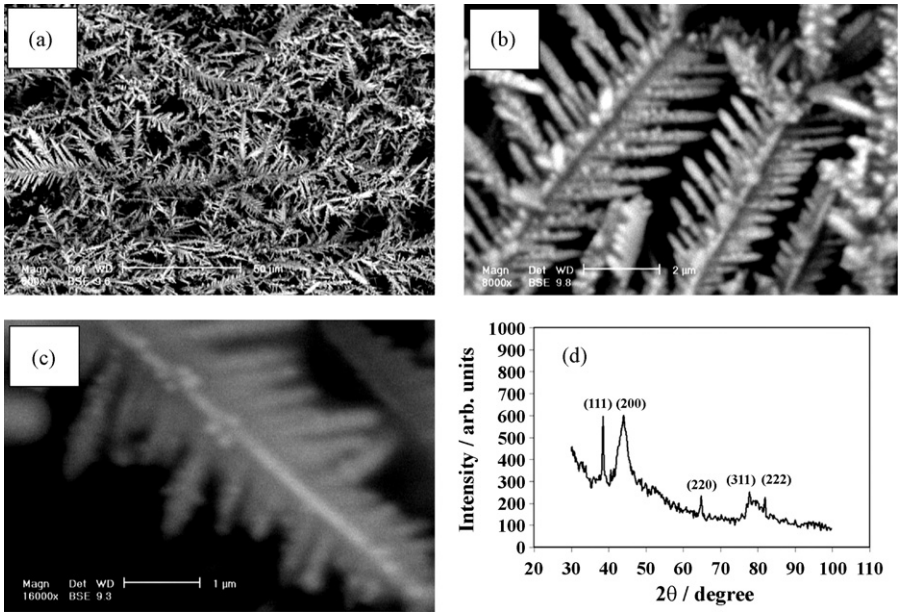

Fig. 1. Typical SEM images of the products obtained for the electrodeposition time of 1200 s at −0.8 V (vs. AgQRE) from a 20.0 mmol L^{-1} $AgNO_3$/(H_2O/PEG, 1:1) solution (a–c). (d) X-ray diffraction (XRD) pattern of AgNDs deposited on the GCE.

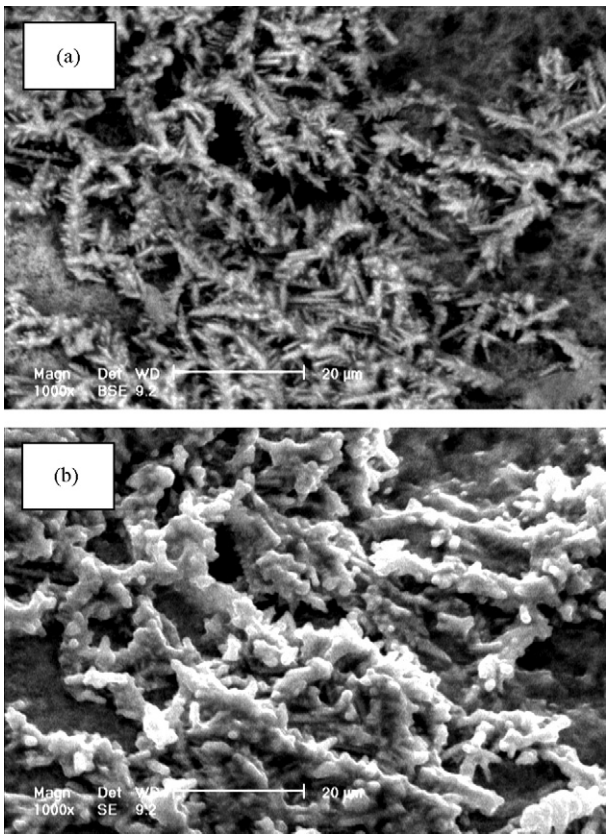

Fig. 2. SEM images of samples synthesized under similar conditions with those of the sample shown in Fig. 1 with only one experimental parameter changed as; (a) applied potentioal: −0.6 V and (b) the PEG-400/H_2O with ratio 1:5 (v:v).

be indexed to diffraction from the (1 1 1), (2 0 0), (2 2 0), (3 1 1), and (2 2 2) of face-centered cubic (fcc) silver crystals. The lattice constant calculated from the XRD pattern is 4.063 Å, a value in agreement with the reported value of a = 4.086 Å from JCPDS 04-0783. Also the distance between interplanar spacing of {1 1 1} planes was determined 0.2321 nm, which is in accordance with the {1 1 1} lattice spacing of fcc Ag (d1 1 1 = 0.2359 nm) [61]. The peaks appear broadened, which implies that the samples are nanocrystalline in nature.

We also investigated the relations between the morphology of silver particles and various experimental parameters including the applied potentials and the concentrations of $AgNO_3$ and PEG-400 as well. Product morphology is largely determined by the applied potential since it decides the electrochemical driving force in the constant potential mode. At the potentials lower than −0.6 V (vs. AgQRE), the density of nanodendritic structures is low, and the dimension of the structures reduce (Fig. 2a), while more dense silver dendrites, with larger dimensions and complex dendrites with numerous side branches are observed when the potential is increased to −0.8 V (see Fig. 1a–c). By changing the potential from −0.6 to −0.8 V, the diameters of the trunk and branches increased from 100 to 300 nm and 40 to 150 nm, respectively. After the potential was further increased to −1.0 V, the uniformity of the products was changed and some high density irregular dendritic silver crystals were formed (not shown).

It is believed that the growth mechanism of the dendritic or tree-like structures follows on the basis of a DLA mode [52,74]. Cluster formation occurs by sticking of particles together with random path on the selected deposited nuclei, allowing the particles to form a growing structure. The used polymer provides significant control over the nucleation and directional aggregation which gives rise to a non-equilibrium system thereby favoring the formation of silver dendrites [75]. Here, the silver precursor is electrochemically reduced to form silver isotropic particles, and they can kinetically coagulate to form anisotropic structures as the concentration of the polymer is increased. The anisotropic silver nanoparticles arrange themselves in a linear shape which provides the reaction environment for the formation of a trunk. Dendritic growth occurs at the tips and stems of branches. As the stem grows in length new shorter branches are formed continuously at the tips. Barkey et al. [76] explained the formation of dendritic morphology based on the anisotropy created by the elementary chemical reaction equilibrium involved in the deposition. However, their case is entirely different from the present case as here the deposition is carried out in a 3D cell unlike theirs, which was carried out in a quasi 2D cell. Here we introduce an interfacial anisotropy by complexing of the Ag^+ in the presence of PEG-400. Initially, interfacial free energy is constant due to the planar substrate surface; however, once the deposition of Ag starts anisotropy is formed for Ag^+/PEG complexes, because the adsorption energy of the complexes may vary drastically depending on the different planes on which the complex is adsorbed compared to the free Ag^+ ions.

In the investigation of parameters, we also observed that the morphology of the resultant particles is very sensitive to the concentrations of $AgNO_3$ and PEG-400. The sample prepared with a low amount of PEG-400 (see Fig. 2b) changed from the dendritic morphology and silver particles were obtained without any well-defined shape. It is quite obvious that PEG-400 is very crucial for the formation of silver dendrites, and it has a structure-directing effect in the electrodeposition process. This could be explained by the fact that on small addition of polymer, large numbers of uncomplexed Ag^+ ions remain in the solution and the Ag^+ ions can get adsorbed and reduced on the substrate surface. Since kinetic anisotropy for the reduction of Ag^+ is much less compared than that of the silver complex, dendritic structures are not observed [26]. The complete complexing of Ag^+ ions with PEG-400 is the most dominant factor in determining the morphology, thus we observe the predominant formation of dendritic morphology in the case of higher additive concentration (see Fig. 1a and b).

In this work, we also used an electrolyte containing higher concentration of Ag^+, 0.05 mol L^{-1} $AgNO_3$ in the PEG-400/H_2O (1:1, v:v), to prepare silver nanomaterials for comparison purpose. The product was deviated from tree-like structure and some microsized silver particles with various shapes along with some high dimension dendrites were formed, almost independent of the applied potential (not shown). This may be due to the fast growth of silver with high concentration of reductive reactants.

In nucleation and growth studies it is also important to determine the grain size, topography of growth, roughness, height of clusters, etc. Such quantitative information may be obtained from the AFM studies. AFM images of silver structures show that after 200 s of electrodeposition at −0.80 V, a large number of small clusters randomly distributed on the GC electrode surface are formed (see Fig. 3A and B). After 1200 s from deposition, the mentioned clusters grow highly in vertical direction with various sizes, as shown in Fig. 3C. The height of nanodendritic clusters increases with time up to about 10 μm in vertical direction with grain size of about 100 nm (see inset (d) of Fig. 3). The main effect of the PEG-400 is to inhibit additional nucleation and to direct vertical and dendritic growth of the metal on the electrode surface. According to the cross sections of AFM images in the insets of Fig. 3, it is observed that by using electrodeposition process in the presence of PEG-400, the growth rate is mainly in the vertical direction and the clusters has been slightly separated.

The density of summits (S_{ds}, the number of peaks per surface area) and the surface roughness parameters of the samples which are expressed in terms of the mean roughness (S_a), the root mean

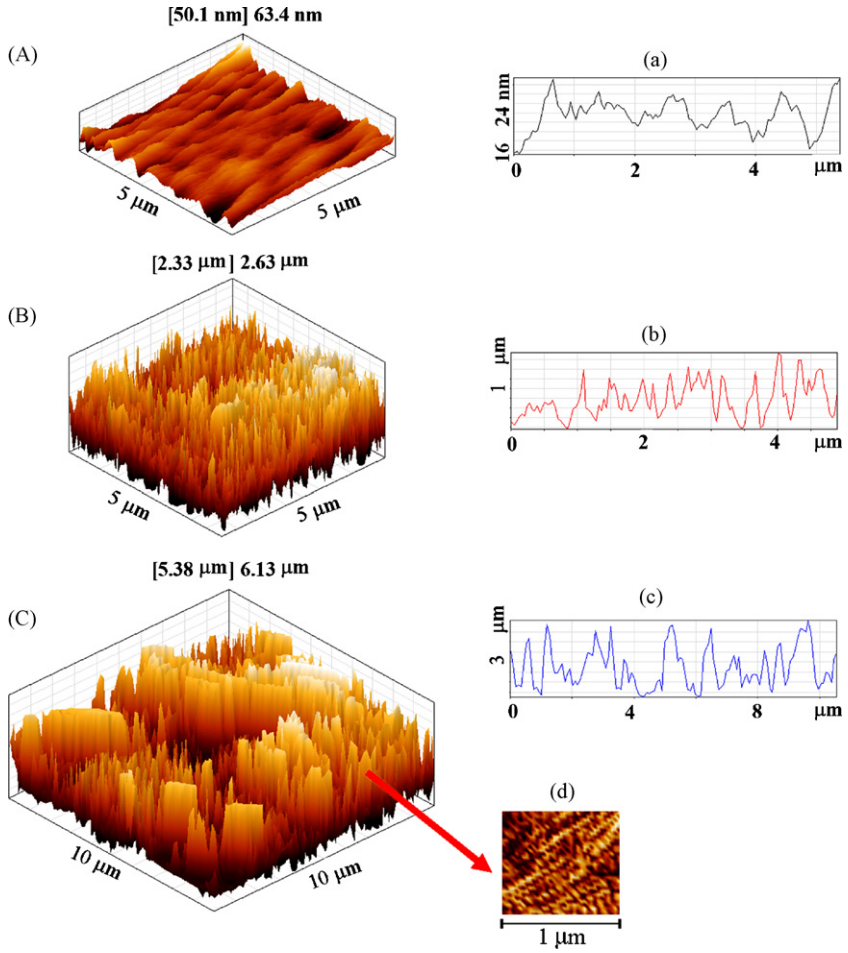

Fig. 3. Three-dimensional AFM images of working electrode after deposition of silver nanoparticles for (A) 0.0 s, (B) 200.0 s, and (C) 1200.0 s at −0.8 V (vs. Ag wire) from a 20.0 mmol L^{-1} $AgNO_3$/(H_2O/PEG, 1:1) solution. Insets (a–c) show typical cross-section lines of AFM profiles, and inset (d) shows a 2D AFM image (1 μm × 1 μm) of AgNDs.

square of the Z data (S_q) and the mean difference between the highest peaks and lowest valleys (S_z) were calculated by SPM software and are presented in Table 1. The roughness parameters for AgNDs increased with the electrodeposition time. Furthermore, a same correlation was also observed between the roughness parameters and the density of summits. The roughness parameters depend on the Z-value, which is the vertical distance that the piezoelectric scanner moves. When the surface includes deep depressions and high peaks, the tip moves up and down over a wide range and the roughness parameter of surface should be high.

The presence of sharp branches and defects on the AgNDs, similar to sharp edges and defects on the carbon nanotubes, which is responsible for their electrocatalytic behaviors, can enhance the electron-transfer kinetics of the electrochemical reactions.

Table 1
Surface roughness parameters of the electrodes extracted from the AFM images mentioned in Fig. 3.

Sample	Roughness parameters			S_{ds}[d] (μm^{-2})
	S_a[a]	S_q[b]	S_z[c]	
A	4.09 nm	5.40 nm	43.05 nm	0.2–1.5
B	1.48 μm	1.85 μm	9.38 μm	6.5–8.0
C	1.84 μm	2.17 μm	10.40 μm	12.0–14.0

[a] The mean roughness (S_a).
[b] The root mean square of the Z data (S_q).
[c] The mean difference between the highest peaks and lowest valleys (S_z).
[d] The number of peaks per surface area (S_{ds}).

3.2. Voltammetric and electrochemical impedance studies

3.2.1. Electrochemical characteristics of the AgNDs electrode

The potentiostatic deposition of silver nanocrystallites on GC electrode was accomplished by applying the potential from 0.0 to −0.8 V vs. AgQRE for 1200 s (see Section 2.3). Representative current–time transient for this electrodeposition is shown in Fig. 4.

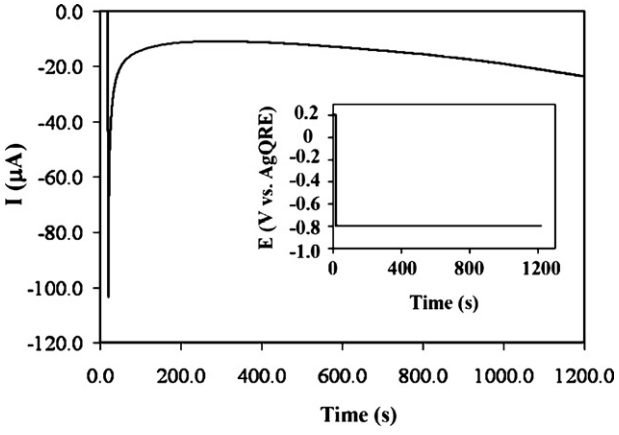

Fig. 4. Current–time transient for the preparation of AgNDs at the constant potential of −0.8 V vs. AgQRE for a period of 20.0 min in the presence of 0.02 mol L^{-1} $AgNO_3$ into a homodisperse mixture of PEG-400/H_2O (1:1, v:v). Inset shows the applied constant potential mode.

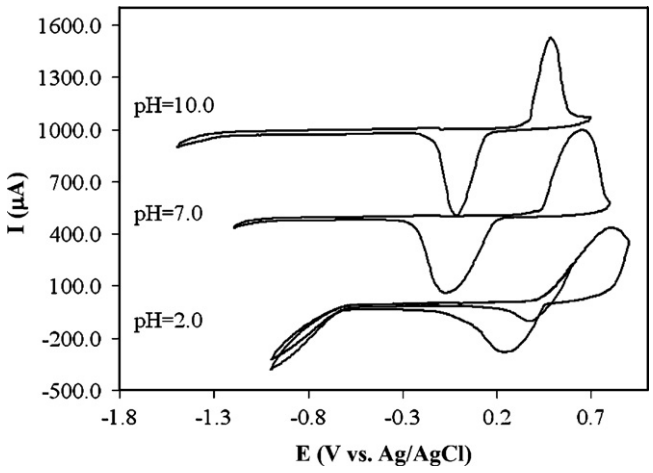

Fig. 5. Cyclic voltammograms of the AgNDs modified GC electrode in the various pHs.

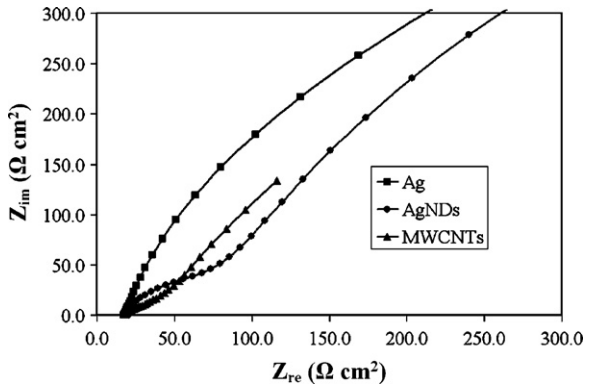

Fig. 6. The Nyquist diagrams of the impedance (Z_{im} vs. Z_{re}) for the bulk Ag, AgNDs and MWCNTs electrodes. Other conditions: 0.1 mmol L^{-1} $K_3[Fe(CN)_6]$ and 0.1 mmol L^{-1} KCl solutions by applying an bias of 0.1 V and ac voltage with 5 mV amplitude in a frequency range from 10.0 Hz to 100.0 kHz.

Silver has been previously shown to be stable on GC and highly ordered pyrolytic graphite electrodes [36,38]. The successive cyclic voltammograms of $AgNO_3$ solution in PEG-400/H_2O (1:1, v:v), with GC as working electrode and an AgQRE as the reference electrode, similar to other reports [38,77], show the characteristic features of the diffusion-controlled electrodeposition in the cathodic branch and stripping of the metal from the electrode surface in the anodic branch. Also, the electrodeposition reaction take place more readily in the second and subsequent scans and their reduction peak is positively shifted with respect to the first scan, due to facilitating the nucleation and deposition process.

The electrochemical behavior of the AgNDs modified GC electrode was characterized by CV and EIS measurements. According to the voltammograms represented in Fig. 5, this electrode shows two sharp, pH dependent redox peaks and the reduction and oxidation peak positions in the universal buffer solution with pH 2.0 were located at +0.2 and +0.8 V, respectively, versus Ag/AgCl. The redox peaks reflect the electrochemical reaction between Ag and Ag_2O/AgO. Two cyclic voltammograms obtained in pH 2.0 condition demonstrate by decreasing the final oxidation potential of silver nanostructures (+0.6 V instead of +0.9 V) the related reduction currents of Ag_2O/AgO considerably diminish, and then the potential window is extended. The potential window of the modified electrode, similar to the conventional Ag electrodes, is limited between the oxidation potential of silver and the hydrogen evolution potential. This pH dependent region having a relatively constant background current is very useful for the sensing applications of the reducible compounds. By increasing the pH of the buffer solution, the AgNDs are oxidized easier but the hydrogen evolution potential increase, that it is provided suitable conditions in the relatively wide pH range for the electroanalysis systems.

The stability of AgNDs modified GC electrodes in the organic and various pH solutions was examined by repetitive voltammetric scanning at the scan rate of 100.0 mV s^{-1} in the basic (pH 10.0), acidic (pH 2.0), neutral (pH 7.0) and organic (acetonitrile) solutions. Relative standard deviations (RSD) of the cathodic background currents at −0.4 V after 50 continuous potential cycling between 0.0 and −0.8 V were 6.3, 1.5, 5.2 and 3.4%, respectively. In the relatively high acidic or basic solutions the AgNDs can gradually be dissolved and demolished. Thus for the electroanalysis applications, it is better to use the AgNDs electrodes in the pH range 5.0–8.0, and to apply potential lower than oxidation region of Ag and before the evolution of hydrogen gas (see Fig. 5), to obtain the best and the stablest conditions.

The electrocatalytic activity of the silver clusters was tested by electrochemical impedance spectroscopy studies using $K_3Fe[CN]_6$ as a redox probe to evaluate the electron-transfer kinetics of the electrodes. Here, the charge transfer resistance of the reactions at AgNDs/GC electrode was compared to the bulk silver and MWCNTs modified GC electrodes. Fig. 6 shows a typical Nyquist plots of the impedance (Ω cm^2) on the mentioned electrodes recorded at +0.1 V as dc-offset for the frequency range of 100.0 kHz–10.0 Hz in the presence of 0.1 mmol L^{-1} HCF and 10.0 mmol L^{-1} KCl solution. The Nyquist plot for this system consists of a semicircle portion observed at higher frequency range corresponding to the electron-transfer-limited process and a linear part at lower frequencies representing the diffusion-limited process. The EIS data were approximated using FRA 4.9 software and complex nonlinear least square (CNLS) approximation method, from which electron-transfer kinetics as charge transfer resistance (R_{ct}), solution resistance (R_s), double layer capacitance (C_{dl}) or constant phase element (*CPE*) and a mass transfer element *W* (Warburg impedance) were extracted. The EIS data obtained for the bulk Ag electrode was fitted to the Randles circuit: $R_s(C[R_{ct}W])$, but for MWCNTs and AgNDs electrodes the modified Randles' model in which C_{dl} was replaced by frequency-dependent constant phase element was used to explain experimental data. By using this method, the electron-transfer resistance, R_{ct}, for the AgNDs modified GC, bulk Ag and MWCNTs electrodes obtained 104.6, 2265.2, and 58.3 Ω cm^2, respectively. The apparent electron-transfer rate constant k_{app} can be obtained from the conventional equation [78]:

$$k_{app} = \frac{RT}{n^2F^2AR_{ct}C} \quad (1)$$

where *n* is the number of electron transferred ($n = 1$), *A* is the microscopic area of the electrodes, *C* is the concentration of the $[Fe(CN)_6]^{3-}$ (in mol cm^{-3}), *R*, *T* and *F* have their usual meanings. Thus, the value of k_{app} for the AgNDs is about 22.0 times higher than that of the bulk Ag electrode, demonstrating enhancement of charge transfer reaction kinetics. Also, the dendritic Ag nanostructures show an electrocatalytic behavior very near to MWCNTs electrodes. This behavior of AgNDs, similar to nanotubes, may be attributed to the presence of very sharp edge sites and nanowires on the tree-like structures. Also on using the electrodes after leaving them unused for period of two-weeks in the ambient conditions the electrocatalytic behavior of AgNDs was again unchanged and the R_{ct} showed only less than 5% decrease of the initial response. The results showed good reproducibility and compared well with those obtained using a freshly prepared electrode. The good stability and repeatability of modified electrode is related to the stability of the silver nanostructures on the GC substrate [36,38] and the

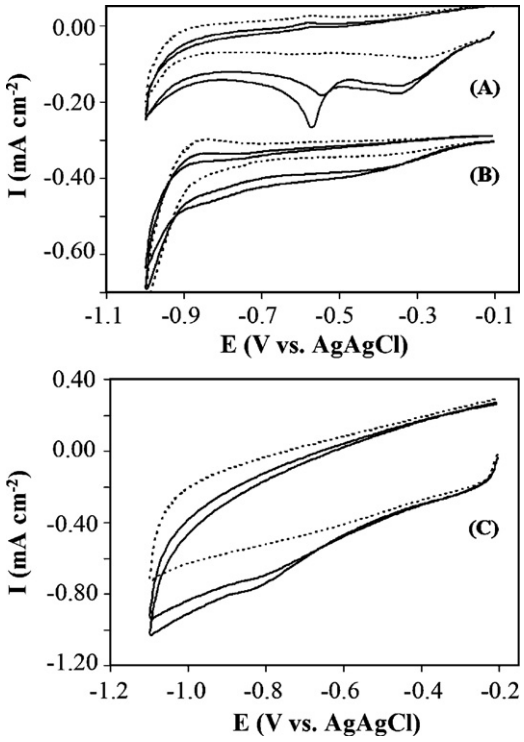

Fig. 7. Cyclic voltammograms of different electrodes in pH 7.0 for the reduction of (a) 0.0 μmol L^{-1}, (b) 100.0 μmol L^{-1}, (c) 100.0 μmol L^{-1} RDX at the scan rate of 100 mV s^{-1} on the (A) AgNDs modified GC, (B) bulk silver and (C) MWCNTs modified GC electrodes.

presence of a little amounts of PEG-400 polymer in the AgNDs that as a coating agent can partly prevent or decrease the oxidation process of dry silver nanostructure. On the other hand, here, the AgNDs electrocatalyst has been used for the reduction process, thus oxidized form of silver on the surface of AgNDs can be electrochemically reduce and convert to metallized Ag. This activation is performed by some cycling the potential on the modified electrode in the negative potential window and in pure buffer solutions until the background current to be constant.

3.2.2. Detection of RDX high explosive on the AgNDs

As a further test of the good electrocatalytic properties of the Ag nanodendrites, cyclic voltammetry is a useful tool to characterize the sensing behavior of the electroactive species on the electrode surface. Fig. 7 illustrates several CVs of 100.0 and 200.0 μmol L^{-1} RDX in pH 7.0 on the three types of electrodes: on the (A) AgNDs coated glassy carbon, (B) conventional bulk Ag and (C) MWCNTs modified GC electrodes. It is observed that AgNDs shows a well-defined stripping peak, while the other two electrodes do not. The electrochemical reaction involves multi-step reduction of the nitro group to hydroxylamines, which subsequently convert to amine groups at more negative potentials [69,79]. This increase in the peak current and the lowering of reduction potential are clear evidences of the catalytic effects of the AgNDs toward the reduction of RDX. This compound has significantly higher electroreduction activity on the Ag electrodes in comparison to MWCNTs or other carbon electrodes. The presence of very high edge and defects on the MWCNTs enhance the redox activity of RDX. On the other hand, the accumulation of this compound on the high specific surface area of AgNDs along with the presence of very high edges and nanowires on this modified electrode leading to significant enhancement of the RDX cathodic current on it. A similar behavior is expected for other reducible species.

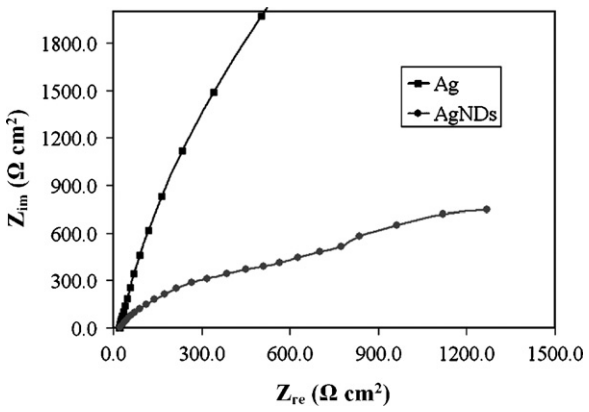

Fig. 8. The impedimetric responses of the bulk Ag and AgNDs/GC electrodes for 100.0 μmol L^{-1} H_2O_2 in the acetonitrile/0.1 mol L^{-1} TBAH solution by applying a bias of −0.3 V and ac voltage with 5 mV amplitude in a frequency range from 10.0 Hz to 100.0 kHz.

In reproducibility tests, it was found that the RSD of the cyclic voltammograms currents of 100.0 μmol L^{-1} RDX (pH 7.0) for ten replicate measurements was 3.8%. To study the reproducibility of the electrode preparation five modified electrodes were prepared, then cyclic voltammograms of 100.0 μmol L^{-1} RDX on them were recorded. Here, the relative standard deviations were found 14.9% (from measurements of cathodic peak currents at −0.58 V). The reason of this deviation is changing of the microscopic surface area of the five different electrodes, so altering the mentioned cathodic currents. By normalizing of the microscopic surface area of the AgNDs electrodes (see Section 2.4), the RSD between the different electrodes reduce to <5.0%.

Long-term stability is one of the most important properties of sensors, biosensors and electrocatalysts. To further test the long-term stability of the Ag clusters under ambient conditions, some cyclic voltammograms for 100.0 μmol L^{-1} RDX were carried out on the modified electrode within a period of ten days. The results were relatively reproducible and compared well with those obtained using a conventional Ag electrode. The average values from ten experiments showed a RSD near to 5.5%. Therefore, no significant aging effect on the electrocatalytic properties of AgNDs/GC emerged from our experiments, at least within a period of ten days.

3.2.3. Performance of the modified electrode in the nonaqueous solutions

The MWCNTs modified GC electrodes shows relatively low physical stability in the organic solvents, and the reported researches about it are limited. But, the metallic nature of the silver nanodendrites on the GC cause to that they have suitable stability in the hydrophobic solutions. The aging and stability of the Ag clusters in the organic conditions was examined by the determination of the cathodic background currents at −0.4 V within a period of ten days after potential cycling between 0.0 and −0.8 V in the acetonitrile solution containing 0.1 mol L^{-1} tetrabutylammonium hexafluorophosphate (TBAH) as the supporting electrolyte. The results showed a <5% decrease in the background currents after ten days. This property offers a useful electrodic material for various electrochemical applications in the organic solution.

In this section, the reduction behavior of H_2O_2 on the bulk Ag and AgNDs modified GC electrodes in the acetonitrile solvent was investigated. Bulk silver has been shown to exhibit catalytic activity for hydrogen peroxide through various pathways, for example autocatalysis and the formation of an oxide layer [4,36]. Fig. 8 shows typical Nyquist plots of the impedance (Ω cm^2) on the mentioned electrodes recorded at −0.3 V as dc-offset in the presence of 100.0 μmol L^{-1} H_2O_2 in acetonitrile solution. It has already

been acknowledged that silver can act catalytically to decompose hydrogen peroxide to water and oxygen [36]. Therefore, the first semicircle seen in the impedance spectrums of Fig. 8 is attributed to the reduction of oxygen, produced via the silver-catalyzed decomposition of hydrogen peroxide. The values of R_{ct} of the first semicircle for the AgNDs and bulk Ag are 1247.4 and 68297.2 $\Omega\,cm^2$, respectively. Thus, the k_{app} on the AgNDs/GC electrode, estimated from the experimental results using Eq. (1), is near to 55.0 times higher than that of bulk Ag electrode, indicating that the nanodendritic structures exhibited very good electrocatalytic activity toward H_2O_2.

4. Conclusion

In this paper, we have used a simple and rapid electrochemical route for the modification of GC electrodes by the silver nanodendrites with well-defined shapes. It is found that electrodeposition time and the concentration of PEG-400 play an important role in controlling the growth morphology of the silver particles. Low concentrations of polymer yield isotropic particles whereas its high concentrations after an extended period give particles in the shape of dendrites. The AgNDs, similar to MWCNTs modified electrodes, significantly improves analytical performances of the corresponding sensors compared to the conventional electrodes. Specifically, the high amounts of sharp edges and defects on the dendrites as electroactive sites along with their large microscopic surface area enhance significantly the electron-transfer rate of the reduction processes compared to conventional bulk Ag electrodes, which is comparable to the electrocatalytic behavior of MWCNTs electrodes. This fabrication method no doubt offers a promising platform for various sensing and biosensing applications, and it may be extended to prepare various useful electrocatalysts with dendritic nanostructures from other noble metals. Also, the results suggest that electrodeposition could be a versatile way to create electrocatalyst with high efficiency and surface area, for various applications such as in the fields of electroanalysis, batteries, fuel cells or other electrochemical systems.

Acknowledgements

The authors wish to thank Isfahan University of Technology (IUT) Research Council and Center of Excellence in Sensor (IUT) for support of this work.

References

[1] A. Eftekhari, Nanostructured Materials in Electrochemistry, Wiley-VCH Verlag GmbH & Co. KGaA, Weinheim, 2008.
[2] A. Wieckowski, E.R. Savinova, C.G. Vayenas, Catalysis and Electrocatalysis at Nanoparticle Surfaces, Marcel Dekker, Inc., New York, 2003.
[3] A. Yu, Z. Liang, J. Cho, F. Caruso, Nano Lett. 3 (2003) 1203.
[4] F.W. Campbell, R.G. Compton, Anal. Bioanal. Chem. 396 (2010) 241.
[5] P. Sun, Anal. Chem. 82 (2010) 276.
[6] C.E. Banks, A. Crossley, C. Salter, S.J. Wilkins, R.G. Compton, Angew. Chem. Int. Ed. 45 (2006) 2533.
[7] B. Rezaei, S. Damiri, Electrochim. Acta 55 (2010) 1801.
[8] X. Luo, A. Morrin, A.J. Killard, M.R. Smyth, Electroanalysis 18 (2006) 319.
[9] J. Wang, Analyst 130 (2005) 421.
[10] M.K. Gupta, N. Sinha, B.K. Singh, N. Singh, K. Kumar, B. Kumar, Mater. Lett. 63 (2009) 1910.
[11] P.L. Taberna, S. Mitra, P. Poizot, P. Simon, J.M. Tar, Nat. Mater. 5 (2006) 567.
[12] M. Conte, P.P. Prosini, S. Passerini, Mater. Sci. Eng. B 108 (2004) 2.
[13] A.L. Andrade, D.M. Souza, M.C. Pereira, J.D.J. Fabris, Nanosci. Nanotechnol. 9 (2009) 3695.
[14] V. Polshettiwar, B. Baruwati, R.S. Varma, ACS Nano 3 (2009) 728.
[15] M. Valcárcel, S. Cárdenas, B.M. Simonet, Anal. Chem. 79 (2007) 4788.
[16] P. Tyagi, D. Postetter, D.L. Saragnese, C.L. Randall, M.A. Mirski, D.H. Gracias, Anal. Chem. 81 (2009) 9979.
[17] M.A. Roberts, S.O. Kelley, J. Am. Chem. Soc. 129 (2007) 11356.
[18] B.K. Jena, C.R. Raj, Langmuir 23 (2007) 4064.
[19] Y.L. Liu, Y.H. Yang, H.F. Yang, Z.M. Liu, G.L. Shen, R.Q. Yu, J. Inorg. Biochem. 99 (2005) 2046.
[20] H.L. Zhang, Y. Zhang, X.G. Zhang, F. Li, C. Liu, J. Tan, H.M. Cheng, Carbon 44 (2006) 2778.
[21] H. Shiigi, R. Morita, Y. Yamamoto, S. Tokonami, H. Nakao, T. Nagaoka, Chem. Commun. 24 (2009) 3615.
[22] J.C. Zhang, L.J. Meng, D.B. Zhao, Z.F. Fei, Q.H. Lu, P.J. Dyson, Langmuir 24 (2008) 2699.
[23] X. Wen, Y.T. Xie, M.W.C. Mak, K.Y. Cheung, X.Y. Li, R. Renneberg, S. Yang, Langmuir 22 (2006) 4836.
[24] Q. Zhou, S. Wang, N. Jia, L. Liu, J. Yang, Z. Jiang, Mater. Lett. 60 (2006) 3789.
[25] X. Wang, K. Naka, H. Itoh, S. Park, Y. Chujo, Chem. Commun. 12 (2002) 1300.
[26] S. Kaniyankandy, J. Nuwad, C. Thinaharan, G.K. Dey, C.G.S. Pillai, Nanotechnology 18 (2007) 125610.
[27] A.D. McFarland, R.P. Van Duyne, Nano Lett. 3 (2003) 1057.
[28] Y.G. Sun, Y.N. Xia, Science 298 (2002) 2176.
[29] Z.Q. Tian, B. Ren, D.Y. Wu, J. Phys. Chem. B 106 (2002) 9463.
[30] C. Shen, C. Hui, T. Yang, C. Xiao, J. Tian, L. Bao, S. Chen, H. Ding, H. Gao, Chem. Mater. 20 (2008) 6939.
[31] Y.G. Sun, Y.N. Xia, J. Am. Chem. Soc. 126 (2004) 3892.
[32] J. Rongchao, C.Y. Charles, H. Encai, G.S. Metraux, G.C. Schatz, C.A. Mirkin, Nature 425 (2003) 487.
[33] Z. Liu, M. Shamsuzzoha, E.T. Ada, W.M. Reichert, D.E. Nikles, J. Power Sources 164 (2007) 472.
[34] S. Park, Y. Xie, M.J. Weaver, Langmuir 18 (2002) 5792.
[35] W.S. Seo, H.H. Jo, K. Lee, B. Kim, S.J. Oh, J.T. Park, Angew. Chem. Int. Ed. 43 (2004) 1115.
[36] C.M. Welch, C.E. Banks, A.O. Simm, R.G. Compton, Anal. Bioanal. Chem. 382 (2005) 12.
[37] B. Zeng, F. Zhao, Fresenius J. Anal. Chem. 369 (2001) 433.
[38] A.A. Isse, S. Gottardello, C. Maccato, A. Gennaro, Electrochem. Commun. 8 (2006) 1707.
[39] B. Zeng, W.C. Purdy, Electroanalysis 10 (1998) 236.
[40] H. Matsuura, Y. Sato, T. Sawaguchi, F. Mizutani, Sensor Actuators B 91 (2003) 148.
[41] L. Trnková, Talanta 56 (2002) 887.
[42] C. Fan, G. Li, Y. Zhuang, J. Zhu, D. Zhu, Electroanalysis 12 (2000) 205.
[43] J. Zhu, Y. Gong, J. Zhang, P. Shen, H. Chert, Electroanalysis 9 (1997) 1030.
[44] J. Wang, R.P. Deo, P. Poulin, M. Mangey, J. Am. Chem. Soc. 125 (2003) 14706.
[45] M. Yang, F. Qu, Y. Lu, Y. He, G. Shen, R. Yu, Biomaterials 27 (2006) 5944.
[46] A.K. Wanekaya, W. Chen, N.V. Myung, A. Mulchandani, Electroanalysis 18 (2006) 533.
[47] Z. Yin, H. Zheng, D. Ma, X. Bao, J. Phys. Chem. C 113 (2009) 1001.
[48] T. Maiyalagan, B. Viswanathan, J. Power Sources 175 (2008) 789.
[49] Z. Jia, J. Liu, Y. Shen, Electrochem. Commun. 9 (2007) 2739.
[50] V. Vamvakaki, K. Tsagaraki, N. Chaniotakis, Anal. Chem. 78 (2006) 5538.
[51] K.A. Dick, K. Deppert, M.W. Larsson, T. Martensson, W. Seifert, L.R. Wallenberg, L. Samuelson, Nat. Mater. 3 (2004) 380.
[52] T.A. Witten, L.M. Sander, Phys. Rev. Lett. 47 (1981) 1400.
[53] B. Jacob, P. Garik, Nature 343 (1990) 523.
[54] S.Z. Wang, H.W. Xin, J. Phys. Chem. 104 (2000) 5681.
[55] Y.C. Zhu, H.G. Zheng, Y.A. Li, Mater. Res. Bull. 38 (2003) 1829.
[56] T. Qiu, X.L. Wu, Y.F. Mei, P.K. Chu, G.G. Siu, Appl. Phys. A 81 (2005) 669.
[57] X.J. Zheng, Z.Y. Jiang, Z.X. Xie, S.H. Zhang, B.W. Mao, L.S. Zheng, Electrochem. Commun. 9 (2007) 629.
[58] Z.H. Kang, E.B. Wang, S.Y. Lian, B.D. Mao, L. Chen, L. Xu, Mater. Lett. 59 (2005) 2289.
[59] J. Zhu, S. Liu, O. Palchik, Y. Koltypin, A. Gedanken, Langmuir 16 (2000) 6396.
[60] Y. Zhou, S.H. Yu, C.Y. Wang, X.G. Li, Y.R. Zhu, Z.Y. Chen, Adv. Mater. 11 (1999) 850.
[61] S. Tang, X. Meng, H. Lu, S. Zhu, Mater. Chem. Phys. 116 (2009) 464.
[62] R. He, X.F. Qian, J. Yin, Z.K. Zhu, Chem. Phys. Lett. 369 (2003) 454.
[63] W. Ye, C. Shen, J. Tian, C. Wang, L. Bao, H. Gao, Electrochem. Commun. 10 (2008) 625.
[64] J. Zhu, X. Liao, H.Y. Chen, Mater. Res. Bull. 36 (2001) 1687.
[65] X. Zheng, L. Zhu, A. Yan, X. Wang, Y. Xie, J. Colloids Interface Sci. 268 (2003) 357.
[66] J. Fang, H. You, P. Kong, Y. Yi, X. Song, B. Ding, Cryst. Growth Des. 7 (2007) 864.
[67] C. Gu, T. Zhang, Langmuir 24 (2008) 12010.
[68] G. Staikov, Electrocrystallization in Nanotechnology, Wiley-VCH Verlag GmbH & Co. KGaA, Weinheim, 2007.
[69] N.P. Saravanan, S. Venugopalan, N. Senthilkumar, P. Santhosh, B. Kavita, H.G. Prabu, Talanta 69 (2006) 656.
[70] B. Rezaei, S. Damiri, IEEE Sens. J. 8 (2008) 1523.
[71] A. Salimi, C.E. Banks, R.G. Compton, Analyst 129 (2004) 225.
[72] S. Smoliński, P. Zelenay, J. Sobkowski, J. Electroanal. Chem. 442 (1998) 41.
[73] B. Baś, M. Jakubowska, Z. Kowalski, Electroanalysis 18 (2006) 1710.
[74] S. Hayashi, R. Koga, M. Ohugi, K. Yamamoto, M. Fujii, Solid State Commun. 76 (1990) 1067.
[75] T. Fukuyo, H. Imai, J. Cryst. Growth 241 (2002) 193.
[76] D. Barkey, F. Oberholtzer, Q. Wu, Phys. Rev. Lett. 75 (1995) 2980.
[77] K.H. Ng, H. Liu, R.M. Penner, Langmuir 16 (2000) 4016.
[78] A.J. Bard, L.R. Faulkner, Electrochemical Methods: Fundamentals and Applications, second ed., John Wiley and Sons, New York, 2001.
[79] S.Y. Ly, D.H. Kim, M.H. Kim, Talanta 58 (2002) 919.